Inorganic Chemistry

Article

pubs.acs.org/IC

Sensitivity of the Valence Structure in Diruthenium Complexes As a Function of Terminal and Bridging Ligands

Abhishek Mandal,[†] Hemlata Agarwala,[†] Ritwika Ray,[†] Sebastian Plebst,[‡] Shaikh M. Mobin,[§] José Luis Priego,[∥] Reyes Jiménez-Aparicio,*[,∥] Wolfgang Kaim,*[,‡] and Goutam Kumar Lahiri*[,†]

[†]Department of Chemistry, Indian Institute of Technology Bombay, Powai, Mumbai 400076, India

[‡]Institut für Anorganische Chemie, Universität Stuttgart, Pfaffenwaldring 55, D-70550 Stuttgart, Germany

[§]Discipline of Chemistry, School of Basic Sciences, Indian Institute of Technology Indore, Indore 452017, India

[∥]Departamento de Química Inorgánica, Facultad de Ciencias Químicas, Universidad Complutense de Madrid, Ciudad Universitaria, E28040 Madrid, Spain

Supporting Information

ABSTRACT: The compounds $[(acac)_2Ru^{III}(\mu\text{-}H_2L^{2-})Ru^{III}(acac)_2]$ (*rac*, **1**, and *meso*, **1′**) and $[(bpy)_2Ru^{II}(\mu\text{-}H_2L^{\bullet-})Ru^{II}(bpy)_2](ClO_4)_3$ (*meso*, $[\mathbf{2}](ClO_4)_3$) have been structurally, magnetically, spectroelectrochemically, and computationally characterized ($acac^-$ = acetylacetonate, bpy = 2,2′-bipyridine, and H_4L = 1,4-diamino-9,10-anthraquinone). The N,O;N′,O′-coordinated $\mu\text{-}H_2L^{n-}$ forms two β-ketiminato-type chelate rings, and **1** or **1′** are connected via NH···O hydrogen bridges in the crystals. **1** exhibits a complex magnetic behavior, while $[\mathbf{2}](ClO_4)_3$ is a radical species with mixed ligand/metal-based spin. The combination of redox noninnocent bridge ($H_2L^0 \rightarrow \rightarrow \rightarrow \rightarrow H_2L^{4-}$) and $\{(acac)_2Ru^{II}\} \rightarrow \rightarrow \{(acac)_2Ru^{IV}\}$ or $\{(bpy)_2Ru^{II}\} \rightarrow \{(bpy)_2Ru^{III}\}$ in **1**/**1′** or **2** generates alternatives regarding the oxidation state formulations for the accessible redox states ($\mathbf{1}^n$ and $\mathbf{2}^n$), which have been assessed by UV−vis−NIR, EPR, and DFT/TD-DFT calculations. The experimental and theoretical studies suggest variable mixing of the frontier orbitals of the metals and the bridge, leading to the following most appropriate oxidation state combinations: $[(acac)_2Ru^{III}(\mu\text{-}H_2L^{\bullet-})Ru^{III}(acac)_2]^+$ ($\mathbf{1}^+$) → $[(acac)_2Ru^{III}(\mu\text{-}H_2L^{2-})Ru^{III}(acac)_2]$ (**1**) → $[(acac)_2Ru^{III}(\mu\text{-}H_2L^{\bullet 3-})Ru^{III}(acac)_2]^-$/$[(acac)_2Ru^{III}(\mu\text{-}H_2L^{2-})Ru^{II}(acac)_2]^-$ ($\mathbf{1}^-$) → $[(acac)_2Ru^{II}(\mu\text{-}H_2L^{4-})Ru^{III}(acac)_2]^{2-}$/$[(acac)_2Ru^{II}(\mu\text{-}H_2L^{2-})Ru^{II}(acac)_2]^{2-}$ ($\mathbf{1}^{2-}$) and $[(bpy)_2Ru^{III}(\mu\text{-}H_2L^{\bullet-})Ru^{II}(bpy)_2]^{4+}$ ($\mathbf{2}^{4+}$) → $[(bpy)_2Ru^{II}(\mu\text{-}H_2L^{\bullet-})Ru^{II}(bpy)_2]^{3+}$/$[(bpy)_2Ru^{II}(\mu\text{-}H_2L^{2-})Ru^{III}(bpy)_2]^{3+}$ ($\mathbf{2}^{3+}$) → $[(bpy)_2Ru^{II}(\mu\text{-}H_2L^{2-})Ru^{II}(bpy)_2]^{2+}$ ($\mathbf{2}^{2+}$). The favoring of Ru^{III} by σ-donating $acac^-$ and of Ru^{II} by the π-accepting bpy coligands shifts the conceivable valence alternatives accordingly. Similarly, the introduction of the NH donor function in H_2L^n as compared to O causes a cathodic shift of redox potentials with corresponding consequences for the valence structure.

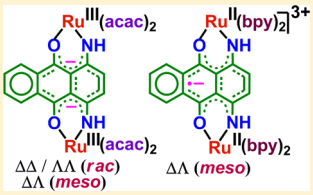

INTRODUCTION

1,4-Disubstituted 9,10-anthraquinones have been widely used as precursor compounds for dyestuffs and as potentially antineoplastic agents of the anthracycline type.[1a] The donor substituents (O or N) at the 1,4 positions may combine with the quinone oxygen atoms to create a bis(chelate) situation with a noninnocent bridge for dimetal coordination. The combination of various accessible valence states of biochemically relevant noninnocent quinonoid systems[1] (Q^0 = quinone, $Q^{\bullet-}$ = semiquinonate, Q^{2-} = catecholate) and of ruthenium (Ru^{II}, Ru^{III}, Ru^{IV}) can result in complex valence and spin distribution patterns at the metal−ligand interface.[2] Close lying and efficiently mixing frontier orbitals are responsible for this behavior, and the high degree of covalent bonding can even preclude specific oxidation state descriptions.[3] The complexity increases significantly when moving from a mononuclear situation to a polynuclear one, creating more variety of reasonable oxidation state alternatives. Indeed, mononuclear[4] and a few polynuclear[5] ruthenium−quinonoid complexes with variegated coordination situations have been explored via experimental investigations and quantum-chemical calculations. These studies revealed a number of interesting electronic structural forms, depending inter alia on the electronic nature of the specific quinonoid framework and on the coligands. The lack of predictability thus emphasizes the need for further scrutiny, particularly with challenging dinuclear molecular systems.

The present article originates as a part of our approach in exploring the electronic structural aspects of oligonuclear quinonoid complexes involving extended π-systems.[5a,b,d,e] It deals with 1,4-diimino-9,10-anthraquinone (H_2L) bridged diruthenium complexes, $\{(AL)_2Ru(\mu\text{-}H_2L)Ru(AL)_2\}^n$, incorporating ancillary ligands (AL) such as electron rich acetylacetonate ($acac^-$) in $\mathbf{1}^n$ and π-accepting 2,2′-bipyridine (bpy) in $\mathbf{2}^n$ (Scheme 1). We report here the synthesis, crystal structure, and magnetic properties of paramagnetic diastereomeric[6] complexes $[(acac)_2Ru^{III}(\mu\text{-}H_2L)Ru^{III}(acac)_2]$ (ΔΔ/ΛΛ, *rac* = **1** and ΔΛ, *meso* = **1′**) and the *meso*-isomer of $[(bpy)_2Ru^{II}(\mu\text{-}H_2L)Ru^{II}(bpy)_2](ClO_4)_3$ ($[\mathbf{2}](ClO_4)_3$). Related compounds re-

Received: February 26, 2014
Published: June 4, 2014

   dx.doi.org/10.1021/ic500452h | *Inorg. Chem.* 2014, 53, 6082−6093

Scheme 1. Representation of Complexes

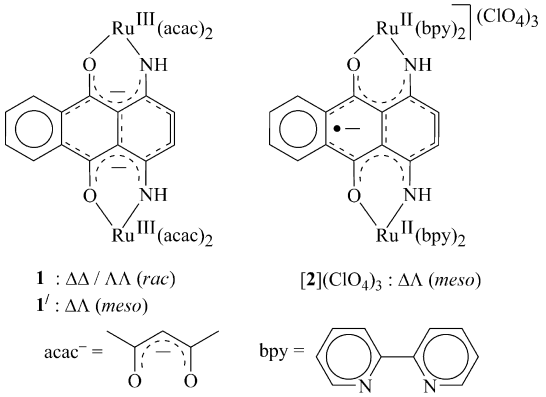

ported were $[(bpy)_2Ru^{II}(\mu\text{-}H_2L)Ru^{III}(bpy)_2](PF_6)_3$,[7] $[(bpy)_2Ru^{II}(\mu\text{-}L')]^+$,[2a] $[(bpy)_2Ru^{II}(\mu\text{-}L'')]^+$,[2b] and $[(acac)_2Ru^{III}(\mu\text{-}QL^{2-})Ru^{III}(acac)_2]$ (**3**)[5d] (HL′ = 1,2-dihydroxy-9,10-anthraquinone, H_2L'' = 1,2-diamino-9,10-anthraquinone, H_2QL = 1,4-dihydroxy-9,10-anthraquinone). The metal−ligand valence and spin state distributions in $\mathbf{1}^n$ (n = 1+, 0, 1−, 2−) and $\mathbf{2}^n$ (n = 4+, 3+, 2+, 1+) have been assessed with special reference to the effect of ancillary ligands via UV−vis−NIR spectroelectrochemistry and EPR in combination with DFT/TD-DFT calculations.

RESULTS AND DISCUSSION

Synthesis and Characterization. Paramagnetic complexes $[(acac)_2Ru^{III}(\mu\text{-}H_2L^{2-})Ru^{III}(acac)_2]$ (*rac* (ΔΔ/ΛΛ), **1**, and *meso* (ΔΛ), **1′**[8]) and $[(bpy)_2Ru^{II}(\mu\text{-}H_2L^{\bullet-})Ru^{II}(bpy)_2](ClO_4)_3$ $[\mathbf{2}](ClO_4)_3$ (*meso* isomer) have been obtained from 1,4-diamino-9,10-anthraquinone (H_4L) and the precursor complexes $Ru^{II}(acac)_2(CH_3CN)_2$ and $[Ru^{II}(bpy)_2(C_2H_5OH)_2]^{2+}$, respectively, in refluxing EtOH and in the presence of NEt_3 as a base, followed by chromatographic purification (Scheme 1).

The neutral diastereomers **1** and **1′** and the 1:3 conducting $[\mathbf{2}](ClO_4)_3$ yielded satisfactory microanalytical and mass spectral data (Experimental Section and Figure S1, Supporting Information). The paramagnetic **1** and **1′** exhibit well-resolved ^1H NMR resonances over a rather wide chemical shift range, from δ = 11.5 to −13.5 ppm in $CDCl_3$ solution at 298 K (Figure S2 and Table S1, Supporting Information), revealing paramagnetic contact shift effects.[5c,d,9a,10] The diastereoisomers **1** and **1′** show slight differences in their chemical shifts (Table S1, Supporting Information). The paramagnetic and EPR-active (cf. below) compound $[\mathbf{2}](ClO_4)_3$ exhibits relatively broad ^1H NMR signals over a chemical shift range from δ = 13 to 5 ppm in CD_3CN solution (Figure S2, Supporting Information).

Crystal Structure. The identity of the diasteroisomeric forms **1**, **1′**, and $[\mathbf{2}](ClO_4)_3$ as *rac*, *meso*, and *meso*, respectively, has been evidenced by their single crystal X-ray structures (Figures 1 and 2). Selected crystallographic parameters, comparative bond lengths, and bond angles are set in Tables 1−3 and Tables S2 and S3 (Supporting Information), respectively.

The presence of metal-coordinated NH groups in the bridge and of negatively charged oxygen atoms of the terminal $acac^-$ ligands creates an opportunity for intermolecular NH···O hydrogen bonding in **1** and **1′**. The corresponding data in Table S4 (Supporting Information) indicate the presence of

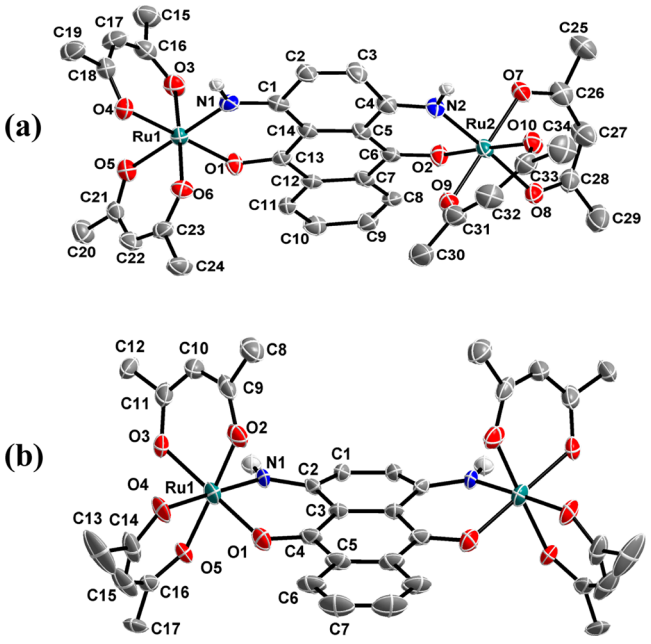

Figure 1. Molecular structures of (a) **1** (*rac*) and (b) **1′** (*meso*). Ellipsoids are drawn at 50% probability level. Hydrogen atoms are removed for clarity.

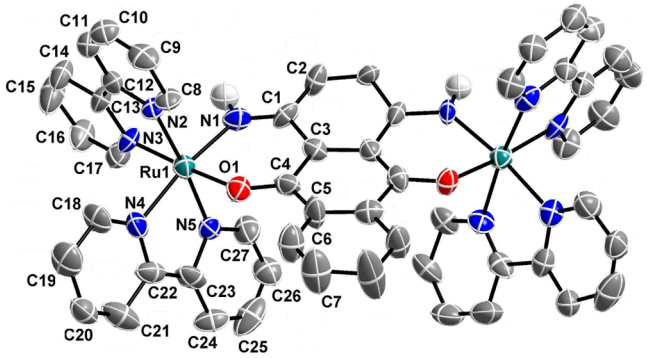

Figure 2. Molecular structure of the complex trication in $[\mathbf{2}](ClO_4)_3$. Ellipsoids are drawn at 50% probability level. Hydrogen atoms are removed for clarity.

such relatively weak hydrogen bonding which may, however, affect the packing of molecules in the crystal.

The two diastereoisomers **1** and **1′** crystallize with largely planar bridging ligands. In both cases, the H_2L^{2-} bridge is linked to two equivalent $\{Ru^{III}(acac)_2\}$ units through O, NH donors for each metal, forming six-membered chelate rings of the β-ketiminato type.[5e,11] The C−O and C−NH bond lengths of coordinated H_2L^{2-} in **1** and **1′** as well as the C−C bond lengths associated with the fused rings confirm this assignment, including the relevance of two resonance forms (Scheme 2).

The Ru−O and Ru−NH distances involving the bridge (H_2L^{2-}) in **1** and **1′** are rather close and the average Ru^{III}−O($acac^-$) bond lengths are in the expected range.[9,12] The average Ru^{III}−O(H_2L^{2-}) bond length in **1** and **1′** is >0.06 Å shorter than the average Ru^{III}−O($acac^-$) distance, implying relatively stronger binding of ruthenium to the bridge. The slightly distorted octahedral features Ru(1)O_5NH and Ru(2)-O_5NH in **1** and **1′** are reflected by the angles around the metal ions (Table S2, Supporting Information). The intramolecular

dx.doi.org/10.1021/ic500452h | Inorg. Chem. 2014, 53, 6082−6093

Table 1. Selected Crystallographic Data for 1, 1′, and $[2](ClO_4)_3$

	1	1′	$[2](ClO_4)_3$
empirical formula	$C_{34}H_{36}N_2O_{10}Ru_2$	$C_{34}H_{36}N_2O_{10}Ru_2$	$C_{54}H_{40}Cl_3N_{10}O_{14}Ru_2$
formula weight	834.79	834.79	1361.45
radiation	Mo Kα	Mo Kα	Cu Kα
crystal system	triclinic	orthorhombic	monoclinic
space group	$P\bar{1}$	*Pnma*	$P2_1/m$
a (Å)	10.8407(5)	15.1800(12)	19.3268(9)
b (Å)	11.9348(6)	17.2648(10)	19.3522(3)
c (Å)	14.6625(6)	14.4310(13)	11.0599(5)
α (deg)	97.885(4)	90	90
β (deg)	107.085(4)	90	132.208(7)
γ (deg)	101.924(4)	90	90
V (Å^3)	1734.04(14)	3782.1(5)	3064.0(2)
Z	2	4	2
μ (mm^{-1})	0.929	0.852	5.782
T (K)	150(2)	150(2)	150(2)
ρ_{calcd} (g cm^{-3})	1.599	1.466	1.476
F (000)	844	1688	1370
θ range (deg)	2.99 to 25.00	2.82 to 25.00	3.84 to 72.32
data/restraints/params	6082/0/441	3434/11/220	6188/0/383
R_1, wR_2 [$I > 2\sigma(I)$]	0.0470, 0.1132	0.1048, 0.2274	0.0506, 0.1436
R_1, wR_2(all data)	0.0614, 0.1254	0.1278, 0.2424	0.0535, 0.1466
GOF on F^2	1.075	1.083	1.037
largest diff in peak and hole (e Å^{-3})	1.763 and −0.862	0.465 and −0.747	2.236 and −0.665

Ru−Ru distance in the *rac* isomer (**1**, 8.123 Å) is slightly longer than that in the *meso* isomer (**1**′, 8.060 Å).

The *meso* diastereoisomeric form of $[2](ClO_4)_3$ has been authenticated by the X-ray structure determination of a solvent-containing single crystal (Figure 2, Tables 1 and 3; Table S3, Supporting Information). Comparison of the bond lengths with those of **1** or **1**′ shows little change, considering the moderate crystal quality.

The Ru−NH and Ru−O bond lengths in $[2](ClO_4)_3$ are distinctly longer than in **1** and **1**′, by about 0.04 Å (Ru−NH) and 0.04−0.06 Å (Ru−O), in agreement with the diminished charge difference (Ru^{II}, $H_2L^{\bullet-}$ versus Ru^{III}, H_2L^{2-}). The average Ru^{II}−N(bpy) distance of 2.060(3) Å in $[2](ClO_4)_3$ is in good agreement with that of reported analogous $\{Ru^{II}(bpy)_2\}$ complexes.[13] The intramolecular Ru−Ru distance in $[2](ClO_4)_3$ is 8.238 Å and thus longer than that in **1** or **1**′. The DFT calculated bond parameters for the optimized **1** and $\mathbf{2}^{3+}$ are in good agreement with the experimental data (Tables 2 and 3; Tables S2, S3 and Figure S3, Supporting Information).

Magnetic Properties. Compounds **1** and $[2](ClO_4)_3$ are paramagnetic at room temperature. Both compounds show dependence of the magnetic properties (magnetic susceptibility and magnetic moment) on the strength of the applied magnetic field (Figures S4 and S5, Supporting Information). In the solid the variation of the magnetic properties with the magnetic field suggests the presence of ferromagnetism. The decrease in magnetic susceptibility and the magnetic moment with the decrease in temperature for **1** and the similar decrease in the magnetic moment for $[2](ClO_4)_3$ can be attributed to antiferromagnetic interactions. These data indicate the simultaneous existence of ferro- and antiferromagnetic interactions in the solid for both complexes. In compound **1** at 1 and 5 T the magnetic susceptibility in the solid becomes negative from 176 to 2 K and 230 to 2 K, respectively, indicating a diamagnetic behavior in these ranges of magnetic field and temperature (Figure S4a, Supporting Information). The diamagnetic behavior at high magnetic field of complex **1** may be due to a magnetic transition from the paramagnetic $S = 1$ state to the diamagnetic $S = 0$ state. Magnetic transitions induced by changing magnetic field strength are well-known in chemistry.[14] In complex $[2](ClO_4)_3$ at 1 and 5 T the variation of the magnetic moment is very small, indicating the presence of only one unpaired electron. The plot of $1/\chi_M$ versus T (Figure S5c, Supporting Information) reveals that at 1 T in the high temperature regime ($T > 50$ K) the compound exhibits Curie−Weiss behavior with the Curie constant 7.07×10^{-6} emu mol^{-1} K and the Weiss constant $\theta = 11.75$ K. The goodness of fit is 99.96. The positive Weiss temperature confirms the existence of ferromagnetic coupling in this sample. Thus, the magnetic data of compound **1** are consistent with a $S = 1$ state at room temperature whereas the data of $[2](ClO_4)_3$ are consistent with a $S = 1/2$ spin state.

Electrochemistry. The diastereomeric complexes **1** and **1**′ exhibit almost identical electrochemical behavior,[5c,d,8] displaying one reversible oxidation (Ox) and two reversible reduction (Red1 and Red2) processes (Figure 3 and Table 4). The one-electron nature of the redox couples has been established by spectroelectroelectrochemistry and EPR. The differences in potentials between the successive redox processes, Ox/Red1 and Red1/Red2 (Figure 3), translate to comproportionation constants of K_{c1} 10^{19} and K_{c2} 10^7, respectively, ($RT \ln K_c = nF(\Delta E)$)[15,16] (Table 4). The corresponding 1,4-dioxido-9,10-anthraquinone bridged bis(2,4-pentanedionato)diruthenium-(III) complex ($[(acac)_2Ru^{III}(\mu\text{-}QL^{2-})Ru^{III}(acac)_2]$, (**3**) exhibits two reversible oxidation and two reversible reduction processes.[5d] The effect of more basic imino groups in the bridge is reflected by a lower oxidation potential and more negative reduction potentials of **1**/**1**′ (Table 4), as compared to the oxido analogue. The analogous mononuclear complexes $Ru(acac)_2(Q)$, Q = phenanthrenequinone-monoimine and *o*-benzoquinoneimine, are reported to undergo reductions at −0.93 V and −0.96 V versus SCE in CH_3CN, respectively.[17]

dx.doi.org/10.1021/ic500452h | *Inorg. Chem.* 2014, 53, 6082−6093

Table 2. Selected Experimental[a] (1, 1′) and DFT Calculated[b] (1) Bond Lengths (Å)

bond length (Å)	1 (expt)[a]	1 (DFT)[b]	1′ (expt)[a]
Ru(1)−N(1)	1.936(4)	1.972	1.940(7)
Ru(1)−O(1)	1.974(3)	2.018	1.983(8)
Ru(1)−O(2)			1.982(8)
Ru(1)−O(3)	2.007(3)	2.041	2.003(8)
Ru(1)−O(4)	2.023(3)	2.066	2.055(7)
Ru(1)−O(5)	2.064(3)	2.098	2.026(8)
Ru(1)−O(6)	2.026(3)	2.059	
Ru(2)−N(2)	1.945(4)	1.971	
Ru(2)−O(2)	1.956(3)	2.016	
Ru(2)−O(7)	2.043(3)	2.047	
Ru(2)−O(8)	2.081(3)	2.095	
Ru(2)−O(9)	2.010(3)	2.049	
Ru(2)−O(10)	2.021(3)	2.077	
C(1)−N(1)	1.314(6)	1.336	
C(2)−N(1)			1.317(10)
C(13)−O(1)	1.282(6)	1.282	
C(4)−O(1)			1.293(11)
C(4)−N(2)	1.316(6)	1.335	
C(6)−O(2)	1.295(6)	1.284	
C(1)−C(2)	1.459(7)	1.444	1.440(11)
C(1)−C(14)	1.453(6)	1.440	
C(2)−C(3)	1.328(7)	1.349	1.444(12)
C(3)−C(4)	1.447(7)	1.444	1.416(13)
C(4)−C(5)	1.445(6)	1.441	1.438(14)
C(5)−C(6)	1.420(6)	1.434	1.390(15)
C(5)−C(14)	1.444(7)	1.464	
C(6)−C(7)	1.464(6)	1.466	1.385(18)
C(7)−C(8)	1.412(6)	1.409	
C(7)−C(12)	1.393(7)	1.407	
C(8)−C(9)	1.379(7)	1.386	
C(9)−C(10)	1.400(7)	1.405	
C(10)−C(11)	1.387(6)	1.386	
C(11)−C(12)	1.398(6)	1.409	
C(12)−C(13)	1.470(6)	1.465	
C(13)−C(14)	1.428(6)	1.435	
C(1)−C(1′)			1.336(16)
C(3)−C(3′)			1.460(18)
C(5)−C(5′)			1.388(2)
C(7)−C(7′)			1.388(3)

[a]From crystal structure analysis of 1 and 1′. [b]UB3LYP level of theory; 6-31G*/LanL2DZ basis sets.

The complex ion $[(bpy)_2Ru^{II}(\mu\text{-}H_2L^{\bullet-})Ru^{II}(bpy)_2]^{3+}$ exhibits one reversible oxidation (Ox) and one such reduction (Red1; Table 4 and Figure 3) with K_c (Ox/Red1) of 10^7, besides bpy-based reductions (Red2 and Red3) at rather negative potentials. Unlike $\mathbf{2}^{3+}$, the corresponding system $\mathbf{4}^n$ was reported to be isolated with the dianionic 1,4-dioxido-9,10-anthraquinone bridging ligand in $[(bpy)_2Ru^{II}(\mu\text{-}QL^{2-})Ru^{II}(bpy)_2]^{2+}$, exhibiting two reversible oxidation and three reversible reduction processes at 0.59 V, 0.86 V and −0.95 V, −1.38 V, −1.73 V, respectively.[18] Relative to oxido substituents the imino groups in the H_2L^n bridge of $\mathbf{2}^{3+}$ thus decrease the oxidation potential and shift the reduction potential to more negative values (Table 4).

MO Analysis by DFT. The variable accessible oxidation states of ruthenium ion ($Ru^{II}/Ru^{III}/Ru^{IV}$) in conjunction with multiple redox steps of noninnocent H_2L^{2-} (Scheme 2) lead to electronic structural alternatives along the accessible redox chain of $\mathbf{1}^n$ or $\mathbf{1}'^n$ (n = 1+, 0, 1−, 2−). As the diastereoisomers **1** and **1′** exhibit almost identical structural and electron-transfer features, the detailed analysis has been performed for **1**, supported by DFT data.

Table 3. Selected Experimental[a] and DFT Calculated[b] Bond Lengths for $\mathbf{2}^{3+}$

bond length (Å)	$\mathbf{2}^{3+}$ (expt)[a]	$\mathbf{2}^{3+}$ (DFT)[b]
Ru(1)−N(1)	1.980(3)	2.030
Ru(1)−O(1)	2.023(3)	2.076
Ru(1)−N(2)	2.056(3)	2.105
Ru(1)−N(3)	2.051(3)	2.097
Ru(1)−N(4)	2.075(3)	2.138
Ru(1)−N(5)	2.059(3)	2.121
C(1)−N(1)	1.313(5)	1.325
C(4)−O(1)	1.291(5)	1.274
C(1)−C(2)	1.448(5)	1.451
C(1)−C(3)	1.464(5)	1.457
C(2)-C(2′)	1.338(8)	1.345
C(3)-C(3′)	1.440(7)	1.442
C(3)−C(4)	1.427(5)	1.452
C(4)−C(5)	1.451(6)	1.466
C(5)−C(6)	1.404(6)	1.407
C(5)-C(5′)	1.407(8)	1.408
C(6)−C(7)	1.380(7)	1.389
C(7)−C(7′)	1.369(12)	1.403

[a]From crystal structure analysis of $[\mathbf{2}](ClO_4)_3$. [b]UB3LYP level of theory; 6-31G*/LanL2DZ basis sets.

Scheme 2. Representation of Different Redox States of H_2L

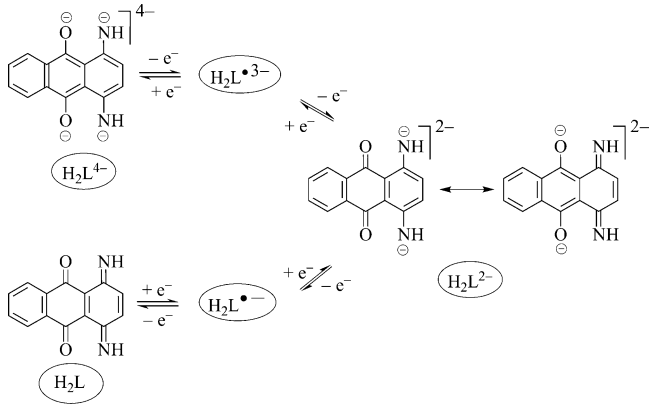

Considering the redox noninnocent behavior of ruthenium and of H_2L^{2-} (Scheme 2), the reversibly electrogenerated species $\mathbf{1}^+$ (or $\mathbf{1}'^+$) can be defined either as a mixed-valent system, $[(acac)_2Ru^{III}(\mu\text{-}H_2L^{2-})Ru^{IV}(acac)_2]^+$, or as a radical bridged homovalent state, $[(acac)_2Ru^{III}(\mu\text{-}H_2L^{\bullet-})Ru^{III}(acac)_2]^+$. However, bridge-dominated singly occupied molecular orbitals (SOMOs) both for **1** (S = 1) (SOMO1: Ru1, 21%, and H_2L, 72%, Table S6, Supporting Information) and for $\mathbf{1}^+$ (S = 3/2) (SOMO1: Ru1, 26%, and H_2L, 55%, Table S7, Supporting Information) as well as the Mulliken spin density distribution of Ru1, 0.861, Ru2, 0.865, and H_2L, 0.804 (Table 5 and Figure 4), for $\mathbf{1}^+$ suggest a mixed situation with $[(acac)_2Ru^{III}(\mu\text{-}H_2L^{\bullet-})Ru^{III}(acac)_2]^+$ and $[(acac)_2Ru^{III}(\mu\text{-}H_2L^{2-})Ru^{IV}(acac)_2]^+$ as major and minor forms, respectively.

The reduction is different: Although the metal dominated β-LUMO of **1** (S = 1), Ru, 68%, and H_2L, 13% (Table S6, Supporting Information), extends an immediate impression of a metal-based first reduction process (Red1, Figure 3), the

dx.doi.org/10.1021/ic500452h | Inorg. Chem. 2014, 53, 6082−6093

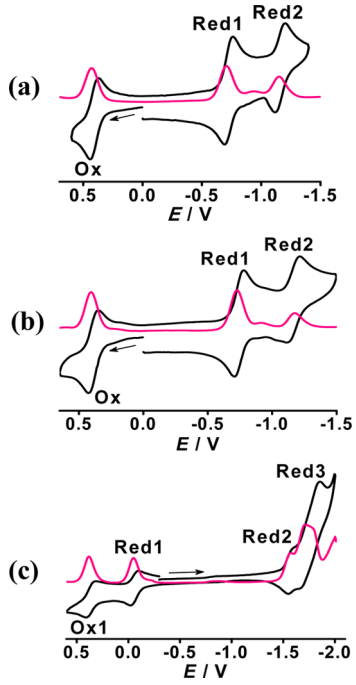

Figure 3. Cyclic voltammograms of (a) **1**, (b) **1′**, and (c) $[\mathbf{2}](ClO_4)_3$ in CH_3CN/0.1 M Et_4NClO_4 versus SCE; scan rate 100 mV s^{-1}.

SOMO composition of $\mathbf{1}^-$ (S = 1/2) (Ru, 39%, and H_2L, 50%, Table S8, Supporting Information) and the Mulliken spin density distribution (Ru1, 0.231, Ru2, 0.219, H_2L, 0.534; Table 5 and Figure 4) imply a resonance situation $[(acac)_2Ru^{III}(\mu\text{-}H_2L^{\bullet 3-})Ru^{III}(acac)_2]^- \leftrightarrow [(acac)_2Ru^{III}(\mu\text{-}H_2L^{2-})Ru^{II}(acac)_2]^-$ for $\mathbf{1}^-$. The MO compositions of $\mathbf{1}^-$ (S = 1/2) (β-LUMO: Ru, 45%, and H_2L, 44%, Table S8, Supporting Information) and $\mathbf{1}^{2-}$ (S = 0) (HOMO: Ru, 36%, and H_2L, 56%, Table S9, Supporting Information) suggest a resonance description $[(acac)_2Ru^{III}(\mu\text{-}H_2L^{4-})Ru^{III}(acac)_2]^{2-} \leftrightarrow [(acac)_2Ru^{II}(\mu\text{-}H_2L^{2-})Ru^{II}(acac)_2]^{2-}$ for the second reduced state (Figure 3, Red2).

The reversibly generated redox states of the analogous 1,4-dioxido-9,10-anthraquinone (QL^{2-}, Scheme 3) bridged complex[5d] $\mathbf{3}^n$ were formulated as $[(acac)_2Ru^{IV}(\mu\text{-}QL^{2-})Ru^{IV}(acac)_2]^{2+}$ (Ox2), $[(acac)_2Ru^{III}(\mu\text{-}QL^{2-})Ru^{IV}(acac)_2]^{2+}$ (Ox1), $[(acac)_2Ru^{III}(\mu\text{-}QL^{3\bullet-})Ru^{III}(acac)_2]^-$ (Red1), and $[(acac)_2Ru^{III}(\mu\text{-}QL^{4-})Ru^{III}(acac)_2]^{2-} \leftrightarrow \{(acac)_2Ru^{II}(\mu\text{-}QL^{2-})Ru^{II}(acac)_2\}^{2-}$ (Red2). Thus, a larger degree of mixing of metal- and bridge-based frontier orbitals has taken place in the imino derivative **1** relative to the oxido analogue.

Bridge-dominated oxidation (Figure 3, Ox) with appreciable metal contribution has been determined for the MO compositions of $\mathbf{2}^{3+}$ (S = 1/2; SOMO: Ru, 31%, and H_2L, 61%, Table S10, Supporting Information) as well as for $\mathbf{2}^{4+}$ (S = 0) (HOMO: Ru, 23%, and H_2L, 71%, Table S11, Supporting Information), leading to the electronic structural forms of $[(bpy)_2Ru^{II}(\mu\text{-}H_2L^{0})Ru^{II}(bpy)_2]^{4+}$ (major contribution)/$[(bpy)_2Ru^{II}(\mu\text{-}H_2L^{\bullet-})Ru^{III}(bpy)_2]^{4+}$ (minor contribution) for $\mathbf{2}^{4+}$. In contrast, the 1,4-dioxido-9,10-anthraquinone bridged

Table 5. DFT Calculated ((U)B3LYP/LanL2DZ/6-31G*) Mulliken Spin Densities

complex	Ru1	Ru2	H_2L	acac[a]/bpy[b]
$\mathbf{1}^+$ (S = 3/2)	0.861	0.865	0.804	0.471
1 (S = 1)	0.740	0.737	0.368	0.154
$\mathbf{1}^-$ (S = 1/2)	0.231	0.219	0.534	0.017
$\mathbf{2}^{3+}$ (S = 1/2)	0.128	0.128	0.752	−0.008
$\mathbf{2}^+$ (S = 1/2)	−0.004	−0.004	−0.002	1.009

[a]For $\mathbf{1}^n$. [b]For $\mathbf{2}^n$.

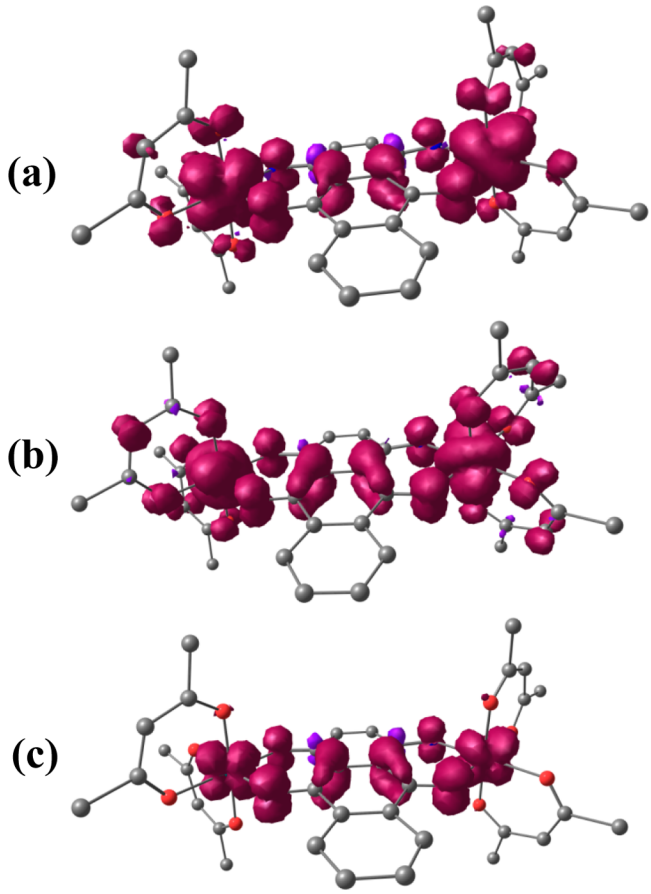

Figure 4. Spin density representations of (a) **1** (S = 1), (b) $\mathbf{1}^+$ (S = 3/2), and (c) $\mathbf{1}^-$ (S = 1/2).

Table 4. Electrochemical Data[a]

	E^0_{298} [V] (ΔE [mV])[b]				K_c[c]		
compd	Ox	Red1	Red2	Red3	K_{c1}[d]	K_{c2}[e]	K_{c3}[f]
1	0.41 (70)	−0.72 (70)	−1.16 (80)		$10^{19.12}$	$10^{7.44}$	
1′	0.39 (70)	−0.74 (70)	−1.17 (90)		$10^{19.12}$	$10^{7.27}$	
$[\mathbf{2}](ClO_4)_3$	0.37 (80)	−0.06 (80)	−1.56 (60)	−1.76 (180)	$10^{7.28}$	$10^{25.38}$	$10^{3.38}$

[a]From cyclic voltammetry in CH_3CN/0.1 M Et_4NClO_4 at 100 mV s^{-1}. [b]Potential in V versus SCE; peak potential differences ΔE [mV] (in parentheses). [c]Comproportionation constant from $RT \ln K_c = nF(\Delta E)$. [d]$K_{c1}$ between Ox and Red1. [e]K_{c2} between Red1 and Red2. [f]K_{c3} between Red2 and Red3.

dx.doi.org/10.1021/ic500452h | Inorg. Chem. 2014, 53, 6082−6093

Scheme 3. Representation of the Ligand QL^{2-}

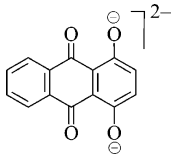

complex $\mathbf{4}^{n}$ was reported to form a mixed-valent $Ru^{II}Ru^{III}$ species.[5d] The first reduction of $\mathbf{2}^{3+}$ (Figure 3c, Red1) also takes place at the bridge, with minor metal contribution (β-LUMO: Ru, 29%, and H_2L, 61%, Table S10, Supporting Information, and HOMO of $\mathbf{2}^{2+}$ ($S = 0$): Ru, 21%, and H_2L, 72%, Table S12, Supporting Information), giving rise to the predominant configuration $[(bpy)_2Ru^{II}(\mu\text{-}H_2L^{2-})Ru^{II}(bpy)_2]^{2+}$ for $\mathbf{2}^{2+}$. As expected, the Red3 process corresponds to a bpy based reduction ($[(bpy)_2Ru^{II}(\mu\text{-}H_2L^{2-})Ru^{II}(bpy)(bpy^{\bullet-})]^{+}$) suggested by the MO composition (LUMO of $\mathbf{2}^{2+}$, 91% bpy, Table S12, Supporting Information, and SOMO of $\mathbf{2}^{+}$ (S = 1/2), 94% bpy, Table S13, Supporting Information) and confirmed by the bpy-based Mulliken spin density of $\mathbf{2}^{+}$ (Table 5 and Figure 5).

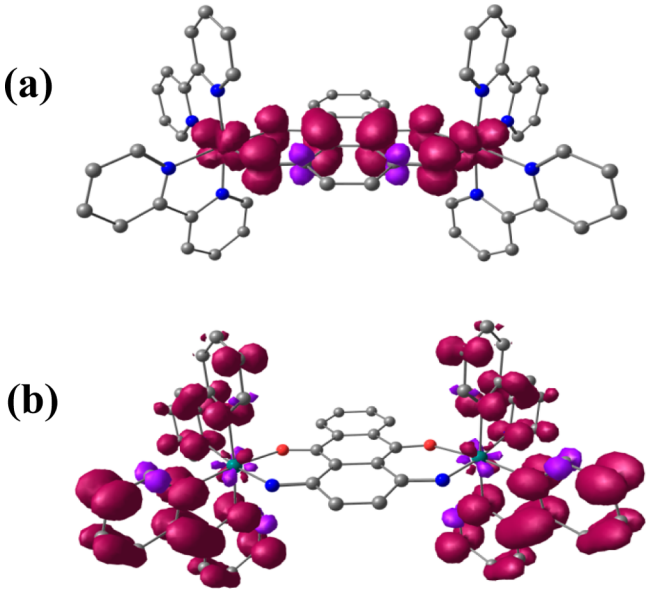

Figure 5. Spin density representations of (a) $\mathbf{2}^{3+}$ (S = 1/2) and (b) $\mathbf{2}^{+}$ (S = 1/2).

EPR Spectroscopy. The neutral complex **1** was studied by EPR in the native state, in the oxidized and in the reduced forms *in situ*, however, no EPR signal was detected under ambient conditions or at low temperature (110 K). Chemical reduction using cobaltocene was also unsuccessful. Relaxation conditions favoring the observation of unbroadened albeit shifted ^{1}H NMR resonance signals as for **1** (Figure S2, Supporting Information) can be expected to disfavor the observation of EPR resonances. According to DFT calculations the one-electron reduction of the $\{Ru^{III}(\mu\text{-}H_2L^{2-})Ru^{III}\}$ precursor leads to a mixed configuration of $\{Ru^{III}(\mu\text{-}H_2L^{\bullet3-})\text{-}Ru^{III}\}$ and $\{Ru^{III}(\mu\text{-}H_2L^{2-})Ru^{II}\}$ for $\mathbf{1}^{-}$ while the oxidation produces a quartet species with a mixture of $\{Ru^{III}(\mu\text{-}H_2L^{\bullet-})Ru^{III}\}$ and $\{Ru^{III}(\mu\text{-}H_2L^{2-})Ru^{IV}\}$ for $\mathbf{1}^{+}$ (Scheme 4); all kinds of such configurations are likely to favor very rapid EPR relaxation through large spin densities on the metal (Figure 4 and Table 5) with its high spin−orbit coupling parameter.[19]

The Mulliken spin density calculations on the DFT optimized lowest energy structures of **1** (S = 1) and $\mathbf{2}^{3+}$ (S = 1/2) (Figure S3 and Table S5, Supporting Information) predict metal (Ru1, 0.740, Ru2, 0.737, H_2L, 0.368) and bridge (Ru1, 0.128, Ru2, 0.128, H_2L, 0.752) dominated spins, respectively (Table 5 and Figures 4,5), corresponding to the electronic structure formulations $[(acac)_2Ru^{III}(\mu\text{-}H_2L^{2-})Ru^{III}(acac)_2]$ (**1**) and $[(bpy)_2Ru^{II}(\mu\text{-}H_2L^{\bullet-})Ru^{II}(bpy)_2]^{3+}$ ($\mathbf{2}^{3+}$).

Taken together with the shifted ^{1}H NMR resonances the absence of an EPR signal for **1** and **1′** (and for $\mathbf{3}$[5d]) agrees with the DFT-calculated S = 1 ground state.

The isolated odd-electron compound $[\mathbf{2}](ClO_4)_3$ (S = 1/2) is paramagnetic with broadened ^{1}H NMR signals; it exhibits a slightly rhombic EPR spectrum in frozen dichloromethane at 110 K (Figure 6). The absence of an EPR signal at room

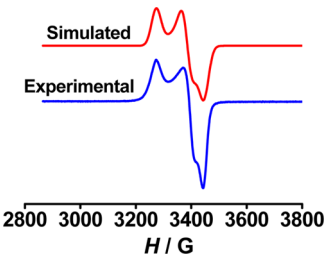

Figure 6. EPR spectrum of $[\mathbf{2}](ClO_4)_3$ in CH_2Cl_2 at 110 K with simulation (for data cf. text).

Scheme 4. Most Appropriate Oxidation State Combinations of $\mathbf{1}^{n}$ and $\mathbf{2}^{n}$ As Deduced from Experimental and Computational Results

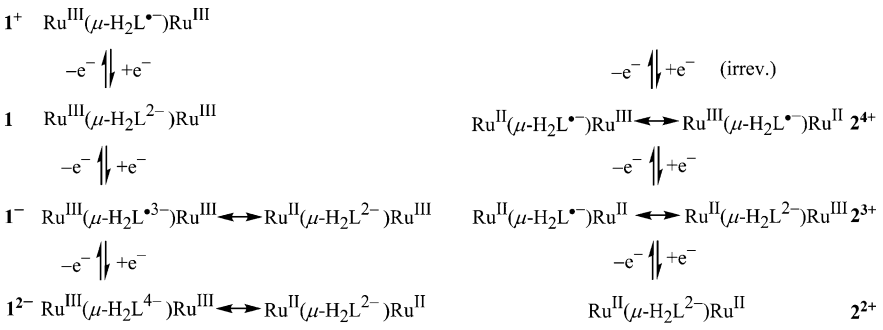

dx.doi.org/10.1021/ic500452h | Inorg. Chem. 2014, 53, 6082−6093

temperature through moderately rapid relaxation and the g component values of $g_1 = 2.0665$, $g_2 = 1.998$, and $g_3 = 1.9625$ indicate a spin distribution with partial but not predominant metal participation. As an approximate guideline for the contributions from ruthenium with its high spin−orbit coupling constant[19] to the singly occupied MO, the anisotropy $\Delta g = g_1 - g_3$ can be used.[4g] The relatively[4g] high Δg value of 0.104 determined here points to an intermediate situation with quite mixed bridging ligand ($[(bpy)_2Ru^{II}(\mu\text{-}H_2L^{\bullet-})Ru^{II}(bpy)_2]^{3+}$) and metal ($[(bpy)_2Ru^{II}(\mu\text{-}H_2L^{2-})Ru^{III}(bpy)_2]^{3+}$) participation at the delocalization of the unpaired electron. Accordingly, the calculation of Mulliken spin densities (Ru1, 0.128, Ru2, 0.128, H_2L, 0.752) in $\mathbf{2}^{3+}$ predicts appreciable spin on the metal ion (Figure 5 and Table 5). Expectedly, the oxidation and reduction of paramagnetic $[\mathbf{2}](ClO_4)_3$ to even-electron species did not produce an EPR signal.

UV−Vis−NIR Spectroelectrochemistry. The spectral features of $\mathbf{1}^n$ (n = 1+, 0, 1−, 2−) and $\mathbf{2}^n$ (n = 4+, 3+, 2+, 1+) as obtained through OTTLE spectroelectrochemistry are shown in Figures 7 and 8 (Table 6), and their analysis is based

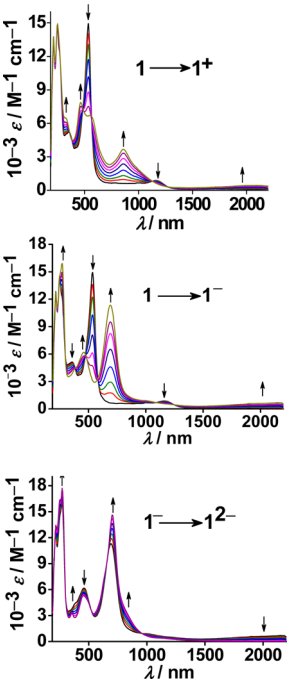

Figure 7. UV−vis−NIR spectroelectrochemistry of $\mathbf{1}^n$ (n = 1+, 0, 1−, 2−) in CH_3CN/0.1 M NBu_4PF_6.

on TD-DFT calculations (Tables 7 and 8). Oxidation of the neutral compound **1** with its $\{Ru^{III}(\mu\text{-}H_2L^{2-})Ru^{III}\}$ configuration results in a diminishing of the weak intraligand ($\pi(H_2L) \rightarrow \pi^*(H_2L)$) band at 1170 nm (TD-DFT: 883 nm) and of the intense LMCT (π(acac) → dπ(Ru))/MLL′CT absorption (dπ(Ru)/π(acac) → $\pi^*(H_2L)$) at 535 nm (TD-DFT: 541/534 nm). A conspicuous new absorption appearing at 860 nm (TD-DFT: 886 nm) and very weak NIR intensity emerging at about 2050 nm (ε = 450 M^{-1} cm^{-1}) for $\mathbf{1}^+$ (TD-DFT: 2881 nm) are assigned to dπ(Ru) → dπ(Ru) and dπ(Ru)/π(acac) → dπ(Ru)/$\pi^*(H_2L)$ transitions, respectively, compatible with the mixed configuration of $\{Ru^{III}(\mu\text{-}H_2L^{\bullet-})Ru^{III}\}/\{Ru^{III}(\mu\text{-}H_2L^{2-})Ru^{IV}\}$. Further oxidation proved to be irreversible in the spectroelectrochemical setup employed.

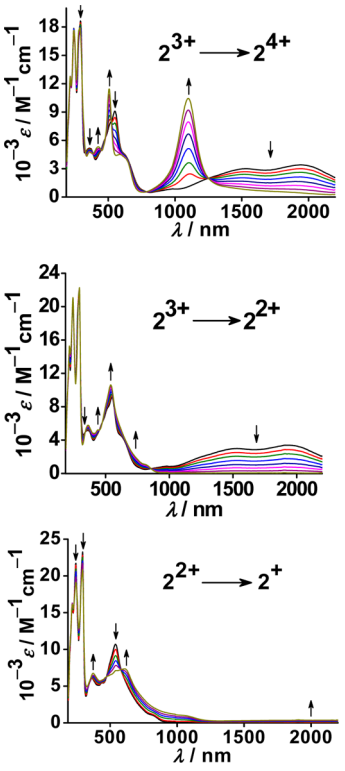

Figure 8. UV−vis−NIR spectroelectrochemistry of $\mathbf{2}^n$ (n = 4+, 3+, 2+, 1+) in CH_3CN/0.1 M NBu_4PF_6.

Table 6. UV−Vis−NIR Spectroelectrochemical Data for $\mathbf{1}^n$, $\mathbf{1}'$, and $\mathbf{2}^n$ in CH_3CN/0.1 M Bu_4NPF_6

$\mathbf{1}^n$/ $\mathbf{2}^n$	λ/nm (ε/M^{-1} cm^{-1})
$\mathbf{1}^+$	250 (14910), 328 (6500), 464 (7900), 550 (6700), 860 (3700), 2050 (450)
1	248 (14820), 270 (sh), 345 (5220), 535 (15000), 1170 (900) {**1**′: 247 (13720), 361 (4300), 538 (11860), 1170 (850)}
$\mathbf{1}^-$	250 (sh), 270 (16000), 382 (sh), 458 (6190), 691 (11330), 990 (sh), 2200 (700)
$\mathbf{1}^{2-}$	248 (sh), 270 (17700), 354 (3260), 453 (5300), 488 (sh), 630 (sh), 704 (14600)
$\mathbf{2}^{4+}$	242 (17750), 287 (17800), 359 (4800), 424 (5300), 530 (11430), 589 (4500), 636 (sh), 1100 (10500)
$\mathbf{2}^{3+}$	243 (17770), 291 (18600), 359 (5190), 512 (sh), 550 (9100), 630 (sh), 1000 (sh), 1530 (3000), 1950 (3400)
$\mathbf{2}^{2+}$	245 (21100), 294 (22200), 364 (5800), 440 (5220), 539 (10600), 820 (sh)
$\mathbf{2}^{+}$	245 (19150), 292 (20900), 372 (6800), 472 (sh), 540 (sh), 606 (7340), 614 (7400), 1078 (sh)

One-electron reduction of **1** results in the occurrence of two MLCT bands in the visible region at 458 and 691 nm (TD-DFT: 450 nm, dπ(Ru) → π^*(acac), and 634 nm, dπ(Ru) → $\pi^*(H_2L)$) while the precursor bands are again diminished. A broad absorption appears in the near IR at about 2200 nm (ε = 700 M^{-1} cm^{-1}) (TD-DFT: 2157 nm, dπ(Ru) → dπ(Ru)/$\pi^*(H_2L)$) which disappears during the second reduction. The NIR feature can be attributed[20] to an intervalence charge transfer (IVCT) transition of a less strongly coupled (class II)[15,21] $\{Ru^{III}(\mu\text{-}H_2L^{2-})Ru^{II}\}$ mixed-valent configuration, mixed with a radical based transition corresponding to the alternative configuration $\{Ru^{III}(\mu\text{-}H_2L^{\bullet 3-})Ru^{III}\}$ for $\mathbf{1}^-$. The doubly reduced form $[(acac)_2Ru^{III}(\mu\text{-}H_2L^{4-})Ru^{III}(acac)_2]^{2-} \leftrightarrow [(acac)_2Ru^{II}(\mu\text{-}H_2L^{2-})Ru^{II}(acac)_2]^{2-}$ ($\mathbf{1}^{2-}$) exhibits an intense

dx.doi.org/10.1021/ic500452h | Inorg. Chem. 2014, 53, 6082−6093

Table 7. Experimental and TD-DFT ((U)B3LYP/CPCM/CH_3CN) Calculated Electronic Transitions for 1^n

λ/nm (expt) (ε/M^{-1} cm^{-1})	λ/nm (DFT) (f)	transitions	character
		$\mathbf{1}^+$ (S = 3/2)	
2050 (450)	2881 (0.001)	HOMO(β) → LUMO+2(β) (0.82)	Ru(dπ)/acac(π) → Ru(dπ)/H_2L(π*)
860 (3700)	886 (0.023)	HOMO-1(β) → LUMO(β) (0.96)	Ru(dπ) → Ru(dπ)
550 (6700)	564 (0.006)	HOMO-7(β) → LUMO+1(β) (0.59)	acac(π) → Ru(dπ)/ H_2L(π*)
464 (7900)	479 (0.007)	HOMO-4(β) → LUMO+2(β) (0.70)	acac(π)/Ru(dπ) → Ru(dπ)/H_2L(π*)
328 (6500)	325 (0.074)	HOMO-6(β) → LUMO+3(β) (0.46)	acac(π) → H_2L(π*)
		$\mathbf{1}$ (S = 1)	
1170 (900)	883 (0.006)	SOMO1(α) → LUMO(α) (0.87)	H_2L(π) → H_2L(π*)
535 (15000)	541 (0.028)	HOMO-5(β) → LUMO(β) (0.55)	acac(π) → Ru(dπ)
345 (5220)	346 (0.010)	HOMO(β) → LUMO+6(β) (0.29) HOMO-1(β) → LUMO+6(β) (0.21)	Ru(dπ) → acac(π*) Ru(dπ) → acac(π*)
		$\mathbf{1}^-$ (S = 1/2)	
2200 (700)	2157 (0.048)	HOMO-1(β) → LUMO(β) (0.88)	Ru(dπ) → Ru(dπ)/H_2L(π*)
691 (11330)	634 (0.040)	HOMO-2(β) → LUMO+1(β) (0.46)	Ru(dπ) → H_2L(π*)
458 (6190)	450 (0.001)	HOMO-2(β) → LUMO+3(β) (0.43)	Ru(dπ) → acac(π*)
		$\mathbf{1}^{2-}$ (S = 0)	
704 (14600)	724 (0.016)	HOMO-2 → LUMO+3 (0.60)	Ru(dπ) → acac(π*)
453 (5300)	470 (0.003)	HOMO-1 → LUMO+2 (0.36) HOMO-3 → LUMO+3 (0.32)	Ru(dπ) → acac(π*) Ru(dπ) → acac(π*)
354 (3260)	357 (0.003)	HOMO-4 → LUMO+4 (0.31)	Ru(dπ) → acac(π*)

Table 8. Experimental and TD-DFT ((U)B3LYP/CPCM/CH_3CN) Calculated Electronic Transitions for 2^n

λ/nm (expt) (ε/M^{-1} cm^{-1})	λ/nm (DFT) (f)	transitions	character
		$\mathbf{2}^{4+}$ (S = 0)	
1100 (10500)	1120 (1.107)	HOMO-1 → LUMO (0.44) HOMO-3 → LUMO (0.42)	Ru(dπ) → Ru(dπ) Ru(dπ) → Ru(dπ)
589 (4500)	567 (0.081)	HOMO-6 → LUMO (0.61)	bpy(π) → Ru(dπ)
530 (11430)	561 (0.255)	HOMO → LUMO+1 (0.54)	H_2L(π) → H_2L(π*)
424 (5300)	427 (0.034)	HOMO-4 → LUMO+1 (0.58)	Ru(dπ)/H_2L(π) → H_2L(π*)
359 (4800)	361 (0.033)	HOMO-20 → LUMO (0.36) HOMO-18 → LUMO (0.32)	bpy(π) → Ru(dπ) bpy(π) → Ru(dπ)
		$\mathbf{2}^{3+}$ (S = 1/2)	
1950 (3400)[a]			
1530 (3000)	1442 (0.197)	HOMO(β) → LUMO(β) (0.94)	Ru(dπ) → H_2L(π*)
1000 (sh)	1065 (0.042)	HOMO-1(β) → LUMO(β) (0.97)	Ru(dπ) → H_2L(π*)
550 (9100)	563 (0.163)	HOMO-1(α) → LUMO(α) (0.69)	Ru(dπ) → H_2L(π*)
359 (5190)	356 (0.018)	HOMO-11(α) → LUMO(α) (0.35)	bpy(π)/H_2L(π) → H_2L(π*)
		$\mathbf{2}^{2+}$ (S = 0)	
539 (10600)	530 (0.143)	HOMO-1 → LUMO+4 (0.48)	Ru(dπ) → H_2L(π*)
440 (5220)	440 (0.006)	HOMO → LUMO+10 (0.63)	H_2L(π) → bpy(π*)
364 (5800)	364 (0.001)	HOMO-1 → LUMO+7 (0.42)	Ru(dπ) → bpy(π*)
		$\mathbf{2}^{+}$ (S = 1/2)	
614 (7400)	613 (0.022)	HOMO-3(α) → LUMO(α) (0.64)	Ru(dπ) → bpy(π*)
606 (7340)	595 (0.039)	SOMO(α) → LUMO+13(α) (0.92)	bpy(π) → H_2L(π*)
372 (6800)	373 (0.010)	HOMO-2(α) → LUMO+6(α) (0.63)	Ru(dπ) → bpy(π*)

[a]See text.

absorption at 704 nm (TD-DFT: 724 nm), followed by a moderately intense band at 453 nm (TD-DFT: 470 nm) corresponding to dπ(Ru) → π*(acac) MLCT transitions, respectively.

Compound $[\mathbf{2}](ClO_4)_3$ with a mixed configuration of $[(bpy)_2Ru^{II}(\mu\text{-}H_2L^{\bullet-})Ru^{II}(bpy)_2]^{3+}$/$[(bpy)_2Ru^{III}(\mu\text{-}H_2L^{2-})\text{-}Ru^{II}(bpy)_2]^{3+}$ is distinguished by moderately intense absorption bands at 1530 and 1950 nm in the near-infrared region beyond 800 nm (TD-DFT: 1442 nm, dπ(Ru) → π*(H_2L)).[22] While the presence of long-wavelength MLCT bands is not unprecedented for radical-bridged diruthenium complexes,[20] the occurrence of two NIR maxima (at 1530 and 1950 nm) is tentatively attributed to the effect of a high spin−orbit coupling constant of the metal, causing forbidden transitions of higher multiplicity to become allowed, as is well established for diosmium systems.[22] EPR spectroscopy has suggested a highly metal/ligand mixed character of the singly occupied MO (SOMO), both radical bridged dinuclear compounds and mixed-valent species can produce near-IR absorptivity.[20] However, TD-DFT calculations suggest that both the NIR and visible (550 nm, TD-DFT: 563 nm) bands involve dπ(Ru) → π*(H_2L) transitions, thus favoring the radical description over the mixed-valent alternative. Ligand-based π(bpy)/π(H_2L) → π*(H_2L) and bpy-targeted dπ(Ru) → π*(bpy) MLCT bands appear in the higher energy region.

Oxidation of $[\mathbf{2}](ClO_4)_3$ to $\{Ru^{II}(\mu\text{-}H_2L^{0})Ru^{II}\}$/$\{Ru^{II}(\mu\text{-}H_2L^{\bullet-})Ru^{III}\}$ yields EPR-silent $\mathbf{2}^{4+}$ which has lost the NIR bands, being replaced by one intense absorption at 1100 nm (TD-DFT: 1120 nm). TD-DFT calculations suggest an MMCT assignment, a dπ(Ru) → dπ(Ru) transition, corre-

dx.doi.org/10.1021/ic500452h | Inorg. Chem. 2014, 53, 6082−6093

sponding to a coupled mixed-valent situation $\{Ru^{II}(\mu\text{-}H_2L^{\bullet-})\text{-}Ru^{III}\}$ with a radical anion bridge as suggested earlier for related cases.[8] Several bands in the visible region between 400 and 600 nm are assigned to intraligand (H_2L) and bpy or H_2L targeted LMCT or MLCT transitions.[23] Further oxidation was found irreversible.

Reduction of $[\mathbf{2}](ClO_4)_3$ is accompanied by the loss of the NIR absorptions. The H_2L^{2-} targeted MLCT ($d\pi(Ru) \rightarrow \pi^*(H_2L)$) transition remains at 539 nm (TD-DFT: 530 nm), together with some weak shoulders. Interligand ($\pi(H_2L) \rightarrow \pi^*(bpy)$) and bpy-directed MLCT transitions ($d\pi(Ru) \rightarrow \pi^*(bpy)$) appear at 440 nm (TD-DFT: 440 nm) and 364 nm (TD-DFT: 364 nm), respectively. An oxidation state formulation $[(bpy)_2Ru^{II}(\mu\text{-}H_2L^{2-})Ru^{II}(bpy)_2]^{2+}$ agrees with these observations made for $\mathbf{2}^{2+}$. The doubly reduced state $[(bpy)_2Ru^{II}(\mu\text{-}H_2L^{2-})Ru^{II}(bpy)(bpy^{\bullet-})]^{+}$ ($\mathbf{2}^{+}$) shows ($d\pi$)Ru $\rightarrow$ (π^*)bpy and (π)bpy $\rightarrow$ (π^*)H_2L transitions at 614 (TD-DFT: 613 nm) and 606 nm (TD-DFT: 595 nm), respectively.

CONCLUSION

Based on experimental and theoretical evidence the oxidation state assignments shown in Scheme 4 have been made. The series of noninnocent ligand-bridged diruthenium redox systems $\mathbf{1}^n$, $\mathbf{1}'^n$, $\mathbf{2}^n$, and $\mathbf{3}^{n5d}$ invites comparisons with regard to different valence distribution:

- The diastereoisomers **1** (*rac*) and **1′** (*meso*) show little spectral and electrochemical difference, as was similarly noted in related cases.
- While the magnetic responses of **1** and **3** are quantitatively different, the $\{Ru^{III}(\mu\text{-}BL^{2-})Ru^{III}\}$ valence description is comparable for both structurally characterized species. The presence of NH functions in **1** and **1′** allows for intermolecular hydrogen bonding.
- The one-electron oxidized forms differ in that the bis(tris(β-diketonato)) species $\mathbf{3}^{+}$ forms a metal-oxidized mixed-valent configuration $Ru^{III}(\mu\text{-}QL^{2-})Ru^{IV}$ with strong IVCT absorption in the near-infrared, whereas the $\mathbf{1}^{+}$ species presented here with the more easily oxidized imine-containing bridge involves a ligand-centered oxidation to $Ru^{III}(\mu\text{-}H_2L^{\bullet-})Ru^{III}$ as confirmed by calculations of the spin density distribution.
- In contrast to the acac-containing diruthenium(III) species **1**, the corresponding bpy-containing state $\mathbf{2}^{4+}$ is distinguished by a very intense near-IR absorption calculated to be a metal-to-metal transition for a radical anion-bridged mixed-valent configuration $Ru^{III}(\mu\text{-}H_2L^{\bullet-})Ru^{II} \leftrightarrow Ru^{II}(\mu\text{-}H_2L^{\bullet-})Ru^{III}$, reflecting the tendency of bpy to stabilize the lower metal oxidation state.
- Another consequence of that $acac^{-}$/bpy difference is observed for the anions which are EPR-silent diruthenium(III) species $Ru^{III}(\mu\text{-}BL^{\bullet3-})Ru^{III}$ for $\mathbf{1}^{-}$, $\mathbf{1}'^{-}$, and $\mathbf{3}^{-}$ whereas the formally corresponding $\mathbf{2}^{3+}$ is structurally and EPR spectroscopically characterized here as a predominantly radical anion complex $Ru^{II}(\mu\text{-}H_2L^{\bullet-})Ru^{II}$, albeit with sizable metal participation.

In contrast to the electron rich $acac^{-}$ which facilitates the stabilization of Ru^{III} in **1** or **1′** as reported for other related cases, the π-accepting bpy ligands favor at least partially Ru^{II} as in $[\mathbf{2}](ClO_4)_3$. However, other than $[(pap)_2Ru^{II}(\mu\text{-}H_2L^{2-})\text{-}Ru^{II}(pap)_2]^{2+}$,[5e] with the strongly π-accepting 2-phenylazopyridine (pap), the isolated ($[\mathbf{2}](ClO_4)_3$) complex contains the anion radical form of the bridge. In an earlier report, this dinuclear $\{Ru(bpy)_2\}$ complex was formulated as a mixed-valent species $[(bpy)_2Ru^{II}(\mu\text{-}H_2L^{2-})Ru^{III}(bpy)_2](PF_6)_3$ based on the low-energy absorption;[7] however, our EPR spectroscopic results clearly rule out this formulation. In summary, the subtly balanced effects of both ancillary and bridging ligands contribute to determine the resulting valence distribution patterns of accessible redox states.

EXPERIMENTAL SECTION

Materials. The precursor complexes $Ru(acac)_2(CH_3CN)_2$[24] and $Ru(bpy)_2Cl_2$[25] were prepared according to procedures reported in the literature. The ligand 1,4-diamino-9,10-anthraquinone was purchased from Alfa Aesar. Other chemicals and solvents were of reagent grade and used as received. For spectroscopic and electrochemical studies HPLC grade solvents were used.

Physical Measurements. Solution electrical conductivities were checked using a Systronic conductivity bridge 305. The EPR measurements were made in a two electrode capillary tube[26] with an X-band (9.5 GHz) Bruker system ESP300 spectrometer. Cyclic voltammetric and differential pulse voltammetric measurements of the complexes in the isolated native state were done using a PAR model 273A electrochemistry system. Platinum wire working and auxiliary electrodes and saturated calomel reference electrode (SCE) were used in a standard three-electrode configuration with tetraethylammonium perchlorate (TEAP) as the supporting electrolyte (substrate concentration $\approx 10^{-3}$ M; standard scan rate 100 mV s^{-1}). ***(Caution!** Perchlorate salts are explosive and should be handled with care.)* UV–vis–NIR spectroelectrochemical studies were performed in CH_3CN/0.1 M Bu_4NPF_6 at 298 K using an optically transparent thin-layer electrode (OTTLE) cell[27] mounted in the sample compartment of a J&M TIDAS spectrophotometer. All spectroelectrochemical experiments were carried out under a dinitrogen atmosphere. The elemental analyses were recorded on a PerkinElmer 240C elemental analyzer. Electrospray mass spectral measurements were done on a Micromass Q-ToF mass spectrometer.

Preparation of Complexes. *$[Ru_2(acac)_4(\mu\text{-}H_2L^{2-})]$, **1** and **1′**.* The starting complex $Ru^{II}(acac)_2(CH_3CN)_2$ (100 mg, 0.26 mmol) and the ligand H_4L (30.97 mg, 0.13 mmol) were taken in 20 mL of ethanol, and then NEt_3 (0.01 mL, 0.07 mmol) was added to the solution followed by refluxing for 6 h. The reaction mixture was evaporated to dryness and purified by using a neutral alumina column. The pure complexes **1** (= *rac* isomer) and **1′** (= *meso* isomer) were eluted by 3:1 CH_2Cl_2–hexane and 6:1 CH_2Cl_2–hexane, respectively. The pure solid products (**1** and **1′**) were obtained on removal of solvent under reduced pressure.

1. Yield: 44 mg (40%). ^1H NMR in $CDCl_3$ [δ/ppm (J/Hz)]: 11.16 (t, 4.04, 2H, H_2L), 8.27 (d, 3.16, 2H, H_2L), 7.29 (s, br, 2H, H_2L), 3.06 (s, 2H, CH(acac)), −1.45 (s, 2H, CH(acac)), 3.39 (s, 6H, CH_3(acac)), 2.54 (s, 6H, CH_3(acac)), 1.10 (s, 6H, CH_3(acac)),0.39 (s, 6H, CH_3(acac)), −12.31 (s, 2H, NH(H_2L)). MS(ESI^+, MeCN): m/z $\{[\mathbf{1}]^+\}$ calcd, 836.04; found, 836.06. Molar conductivity (MeCN): $\Lambda_M = 2\ \Omega^{-1}\ cm^2\ M^{-1}$. Anal. Calcd for $C_{34}H_{36}N_2O_{10}Ru_2$: C, 48.92; H, 4.35; N, 3.36. Found: C, 48.70; H, 4.33; N, 3.20.

1′. Yield: 35 mg (32%). ^1H NMR in $CDCl_3$ [δ/ppm (J/Hz)]: 11.18 (s, br, 2H, H_2L), 8.28 (d, 3.12, 2H, H_2L), 7.20 (s, br, 2H, H_2L), 3.19 (s, 2H, CH(acac)), −1.12 (s, 2H, CH(acac)), 3.24 (s, 6H, CH_3(acac)), 2.47 (s, 6H, CH_3(acac)), 1.18 (s, 6H, CH_3(acac)), 0.48 (s, 6H, CH_3(acac)), −13.10 (s, 2H, NH(H_2L)). MS(ESI^+, MeCN): m/z $\{[\mathbf{1}']^+\}$ calcd, 836.04; found, 836.05. Molar conductivity (MeCN): $\Lambda_M = 4\ \Omega^{-1}\ cm^2\ M^{-1}$. Anal. Calcd for $C_{34}H_{36}N_2O_{10}Ru_2$: C, 48.92; H, 4.35; N, 3.36. Found: C, 48.75; H, 4.31; N, 3.22.

$[Ru_2(bpy)_4(\mu\text{-}H_2L^{2-})](ClO_4)_3$, $[\mathbf{2}](ClO_4)_3$. The starting complex $Ru(bpy)_2(Cl)_2$ (100 mg, 0.21 mmol) and $AgClO_4$ (87.07 mg, 0.42 mmol) were taken in EtOH and refluxed for 2 h. The precipitated AgCl was filtered off through a sintered Gooch crucible. The filtrate was taken in a two-necked round-bottomed flask, and the ligand H_4L (25.01 mg, 0.105 mmol) and NEt_3 (0.007 mL, 0.05 mmol) were added to it. The mixture was refluxed for 6 h. The solvent was evaporated to dryness under reduced pressure. The dry mass was moistened with a

dx.doi.org/10.1021/ic500452h | Inorg. Chem. 2014, 53, 6082–6093

few drops of CH_3CN followed by the addition of saturated aqueous $NaClO_4$ solution to it. It was then chilled overnight. The solid mass thus obtained was filtered off, washed with chilled water to remove the excess $NaClO_4$, and dried in vacuo over P_4O_{10}. It was purified by using a neutral alumina column and 6:1 $CH_3CN-CH_2Cl_2$ mixture as an eluant. The solvent was removed under reduced pressure, which yielded the pure solid mass of $[\mathbf{2}](ClO_4)_3$. Yield: 107 mg (75%). MS(ESI$^+$, MeCN): m/z $\{[\mathbf{2}](ClO_4)_2\}^+$ calcd, 1262.04; found, 1262.06. Molar conductivity (MeCN): $\Lambda_M = 290\ \Omega^{-1}\ cm^2\ M^{-1}$. Anal. Calcd for $C_{54}H_{40}N_{10}O_{14}Cl_3Ru_2$: C, 47.64; H, 2.96; N, 10.29. Found: C, 47.36; H, 2.94; N, 10.38.

Crystal Structure Determination. Single crystals were grown by slow diffusion of CH_3OH vapor into the $CHCl_3$ solution of **1**, and slow evaporation of 1:3 CH_2Cl_2–hexane and 1:4 CH_3CN–toluene solutions of **1′** and $[\mathbf{2}](ClO_4)_3$, respectively. X-ray diffraction data were collected using a CCD Agilent Technologies (Oxford Diffraction) SUPER NOVA diffractometer. The data were collected by the standard phi-omega scan techniques, and were scaled and reduced using CrysAlisPro RED software. The structure was solved by direct method using SHELXS-97 and refined by full matrix least-squares with SHELXL-97, refining on F^2.[28] All non-hydrogen atoms were refined anisotropically. The remaining hydrogen atoms were placed in geometrically constrained positions and refined with isotropic temperature factors, generally $1.2U_{eq}$ of their parent atoms. Hydrogen atoms were included in the refinement process as per the riding model. SQUEEZE was applied for the highly disordered two water molecules in the crystal of $[\mathbf{2}](ClO_4)_3$.

Magnetism. The variable-temperature magnetic susceptibilities were measured on polycrystalline samples with a Quantum Design MPMSXL SQUID (superconducting quantum interference device) susceptometer over a temperature range of 2 to 300 K at the constant field of 0.1 T, 1 T, and 5 T. Each raw data set was corrected for the diamagnetic contribution of both the sample holder and the complex to the susceptibility. The molar diamagnetic corrections were calculated on the basis of Pascal constants.

Computational Details. Full geometry optimizations were carried out using the density functional theory method at the (U)B3LYP level for $\mathbf{1}^+$, **1**, $\mathbf{1}^-$, $\mathbf{2}^{3+}$, and $\mathbf{2}^+$ and (R)B3LYP for $\mathbf{1}^{2-}$, $\mathbf{2}^{4+}$, and $\mathbf{2}^{2+}$.[29] All elements except ruthenium were assigned the 6-31G(d) basis set. The LanL2DZ basis set with effective core potential was employed for the ruthenium atom.[30] Vibrational frequency calculations were performed to ensure that the optimized geometries represent the local minima and there are only positive eigenvalues. All calculations were performed with the Gaussian09 program package.[31] Vertical electronic excitations based on B3LYP optimized geometries were computed for $\mathbf{1}^+$, **1**, $\mathbf{1}^-$, $\mathbf{1}^{2-}$, $\mathbf{2}^{4+}$, $\mathbf{2}^{3+}$, $\mathbf{2}^{2+}$, and $\mathbf{2}^+$ using the time-dependent density functional theory (TD-DFT) formalism[32] in acetonitrile using the conductor-like polarizable continuum model (CPCM).[33] Chemissian 1.7[34] was used to calculate the fractional contributions of various groups to each molecular orbital. All the calculated structures were visualized with ChemCraft.[35]

■ ASSOCIATED CONTENT

Supporting Information

X-ray crystallographic files in CIF format for *rac*-**1**, *meso*-**1′**, and *meso*-$[\mathbf{2}](ClO_4)_3$, mass spectra (Figure S1), ^{1}H NMR (Figure S2, Table S1), magnetic data (Figures S4, S5), crystal data (Tables S2, S3), hydrogen bonding parameters (Table S4), DFT data set for $\mathbf{1}^n$ and $\mathbf{2}^n$ (Figure S3, Tables S5–S13). This material is available free of charge via the Internet at http://pubs.acs.org. CCDC-978230 (**1**), -978231 (**1′**), and -978232 ($[\mathbf{2}](ClO_4)_3$) contain supplementary crystallographic data for this paper. These data can be obtained free of charge from The Cambridge Crystallographic Data Centre via www.ccdc.cam.ac.uk/data_request/cif.

■ AUTHOR INFORMATION

Corresponding Authors

*E-mail: lahiri@chem.iitb.ac.in (G.K.L).
*E-mail: kaim@iac.uni-stuttgart.de (W.K.).
*E-mail: reyesja@quim.ucm.es (R.J.-A.).

Notes

The authors declare no competing financial interest.

■ ACKNOWLEDGMENTS

Financial support received from the Department of Science and Technology and the Council of Scientific and Industrial Research (fellowship to A.M. and H.A.), the University Grants Commission (fellowship to R.R.), New Delhi (India), the DAAD, FCI, and DFG (Germany), and the Spanish Ministerio de Economía y Competitividad (CTQ2011-23066) and Comunidad de Madrid (S2009/MAT-1467) is gratefully acknowledged.

■ REFERENCES

(1) (a) Lown, J. W. *Pharmacol. Ther.* **1993**, *60*, 185–214. (b) Duine, J. A.; Jongejan, J. A. In *Bioinorganic Catalysis*; Reedijk, J., Ed.; Marcel Dekker: New York, 1993; p 447. (c) Klinman, J. P. *Proc. Natl. Acad. Sci. U.S.A.* **2001**, *98*, 14766–14768. (d) Mure, M.; Mills, S. A.; Klinman, J. P. *Biochemistry* **2002**, *41*, 9269–9278. (e) Klinman, J. P.; Bonnot, F. *Chem. Rev.* **2014**, *114* (8), 4343–4365. (f) Mure, M.; Wang, S. X.; Klinman, J. P. *J. Am. Chem. Soc.* **2003**, *125*, 6113–6125. (g) Anthony, C. *Arch. Biochem. Biophys.* **2004**, *428*, 2–9. (h) Anthony, C. *Biochem. J.* **1996**, *320*, 697–711. (i) He, M.; Sheldon, P. J.; Sherman, D. H. *Proc. Natl. Acad. Sci. U.S.A.* **2001**, *98*, 926–931.

(2) (a) DelMedico, A.; Dodsworth, E. S.; Lever, A. B. P.; Pietro, W. J. *Inorg. Chem.* **2004**, *43*, 2654–2671. (b) da Cunha, C. J.; Dodsworth, E. S.; Monteiro, M. A.; Lever, A. B. P. *Inorg. Chem.* **1999**, *38*, 5399–5409.

(3) Remenyi, C.; Kaupp, M. *J. Am. Chem. Soc.* **2005**, *127*, 11399–11413.

(4) (a) Das, A. K.; Hübner, R.; Sarkar, B.; Fiedler, J.; Záliš, S.; Lahiri, G. K.; Kaim, W. *Dalton Trans.* **2012**, *41*, 8913–8921. (b) Das, D.; Mondal, T. K.; Chowdhury, A. D.; Weisser, F.; Schweinfurth, D.; Sarkar, B.; Mobin, S. M.; Urbanos, F. A.; Jiménez-Aparicio, R.; Lahiri, G. K. *Dalton Trans.* **2011**, *40*, 8377–8390. (c) Agarwala, H.; Das, D.; Mobin, S. M.; Mondal, T. K.; Lahiri, G. K. *Inorg. Chim. Acta* **2011**, *374*, 216–225. (d) Das, D.; Sarkar, B.; Kumbhakar, D.; Mondal, T. K.; Mobin, S. M.; Fiedler, J.; Urbanos, F. A.; Jiménez-Aparicio, R.; Kaim, W.; Lahiri, G. K. *Chem.—Eur. J.* **2011**, *17*, 11030–11040. (e) Das, D.; Mondal, T. K.; Mobin, S. M.; Lahiri, G. K. *Inorg. Chem.* **2009**, *48*, 9800–9810. (f) Das, D.; Das, A. K.; Sarkar, B.; Mondal, T. K.; Mobin, S. M.; Fiedler, J.; Záliš, S.; Urbanos, F. A.; Jiménez-Aparicio, R.; Kaim, W.; Lahiri, G. K. *Inorg. Chem.* **2009**, *48*, 11853–11864. (g) Patra, S.; Sarkar, B.; Mobin, S. M.; Kaim, W.; Lahiri, G. K. *Inorg. Chem.* **2003**, *43*, 6469–6473. (h) Maji, S.; Patra, S.; Chakraborty, S.; Mobin, S. M.; Janardanan, D.; Sunoj, R. B.; Lahiri, G. K. *Eur. J. Inorg. Chem.* **2007**, 314–323. (i) Bag, N.; Lahiri, G. K.; Basu, P.; Chakravorty, A. *J. Chem. Soc., Dalton Trans.* **1992**, 113–117. (j) Bag, N.; Pramanik, A.; Lahiri, G. K.; Chakravorty, A. *Inorg. Chem.* **1992**, *31*, 40–45. (k) Ebadi, M.; Lever, A. B. P. *Inorg. Chem.* **1999**, *38*, 467–474. (l) Metcalfe, R. A.; Lever, A. B. P. *Inorg. Chem.* **1997**, *36*, 4762–4771. (m) Masui, H.; Lever, A. B. P.; Dodsworth, E. S. *Inorg. Chem.* **1993**, *32*, 258–267. (n) Schwederski, B.; Kaim, W. *Inorg. Chim. Acta* **1992**, *195*, 123–126. (o) Masui, H.; Lever, A. B. P.; Auburn, P. *Inorg. Chem.* **1991**, *30*, 2402–2410. (p) Haga, M.; Dodsworth, E. S.; Lever, A. B. P. *Inorg. Chem.* **1986**, *25*, 447–453. (q) Salmonsen, R. B.; Abelleira, A.; Clarke, M. J. *Inorg. Chem.* **1984**, *23*, 385–387. (r) Waldhör, E.; Schwederski, B.; Kaim, W. *J. Chem. Soc., Perkin Trans. 2* **1993**, 2109–2111. (s) Pierpont, C. G. *Coord. Chem. Rev.* **2001**, *219–221*, 415–433. (t) Pierpont, C. G.; Attia, A. S. *Collect. Czech. Chem. Commun.* **2001**, *66*, 33–51. (u) Pierpont, C. G.; Lange, C. W. *Prog. Inorg. Chem.* **1994**, *41*, 331–442. (v) Dei, A.; Gatteschi, D.; Sangregorio, C.; Sorace, L.

Acc. Chem. Res. **2004**, *37*, 827−835. (w) Lever, A. B. P.; Gorelsky, S. I. *Coord. Chem. Rev.* **2000**, *208*, 153−167. (x) Bhattacharya, S. *Polyhedron* **1994**, *13*, 451−456. (y) Kurihara, M.; Daniele, S.; Tsuge, K.; Sugimoto, H.; Tanaka, K. *Bull. Chem. Soc. Jpn.* **1998**, *71*, 867−875. (z) Gorelsky, S. I.; Lever, A. B. P.; Ebadi, M. *Coord. Chem. Rev.* **2002**, *230*, 97−105.

(5) (a) Kumbhakar, D.; Sarkar, B.; Das, A.; Das, A. K.; Mobin, S. M.; Fiedler, J.; Kaim, W.; Lahiri, G. K. *Dalton Trans.* **2009**, *43*, 9645−9652. (b) Ghumaan, S.; Sarkar, B.; Maji, S.; Puranik, V. G.; Fiedler, J.; Urbanos, F. A.; Jiménez-Aparicio, R.; Kaim, W.; Lahiri, G. K. *Chem.—Eur. J.* **2008**, *14*, 10816−10828. (c) Kumbhakar, D.; Sarkar, B.; Maji, S.; Mobin, S. M.; Fiedler, J.; Urbanos, F. A.; Jiménez-Aparicio, R.; Kaim, W.; Lahiri, G. K. *J. Am. Chem. Soc.* **2008**, *130*, 17575−17583. (d) Maji, S.; Sarkar, B.; Mobin, S. M.; Fiedler, J.; Urbanos, F. A.; Jimenez-Aparicio, R.; Kaim, W.; Lahiri, G. K. *Inorg. Chem.* **2008**, *47*, 5204−5211. (e) Ghumaan, S.; Mukherjee, S.; Kar, S.; Roy, D.; Mobin, S. M.; Sunoj, R. B.; Lahiri, G. K. *Eur. J. Inorg. Chem.* **2006**, 4426−4441. (f) Kar, S.; Sarkar, B.; Ghumaan, S.; Janardanan, D.; van Slageren, J.; Fiedlar, J.; Puranik, V. G.; Sunoj, R. V.; Kaim, W.; Lahiri, G. K. *Chem.—Eur. J.* **2005**, *11*, 4901−4911. (g) Patra, S.; Sarkar, B.; Ghumaan, S.; Fiedler, J.; Zalis, S.; Kaim, W.; Lahiri, G. K. *Dalton Trans.* **2004**, 750−753. (h) Chakarborty, S.; Laye, R. H.; Paul, R. L.; Gonnade, R. G.; Puranik, V. G.; Ward, M. D.; Lahiri, G. K. *J. Chem. Soc., Dalton Trans.* **2002**, 1172−1179. (i) Ghumaan, S.; Sarkar, B.; Patra, S.; van Slageren, J.; Fiedler, J.; Kaim, W.; Lahiri, G. K. *Inorg. Chem.* **2005**, *45*, 3210−3214. (j) Braunstein, P.; Demessence, A.; Siri, O.; Taquet, J.-P. *C. R. Chim.* **2004**, *7*, 909−913. (k) Masui, H.; Freda, A. L.; Zerner, M. C.; Lever, A. B. P. *Inorg. Chem.* **2000**, *39*, 141−152. (l) Ernst, S.; Hänel, P.; Jordanov, J.; Kaim, W.; Kasack, V.; Roth, E. *J. Am. Chem. Soc.* **1989**, *111*, 1733−1738. (m) Ernst, S.; Kasack, V.; Bessenbacher, C.; Kaim, W. *Z. Naturforsch.* **1987**, *42b*, 425−430. (n) Ward, M. D.; McCleverty, J. A. *J. Chem. Soc., Dalton Trans.* **2002**, 275−288. (o) Kasack, V.; Kaim, W.; Binder, H.; Jordanov, J.; Roth, E. *Inorg. Chem.* **1995**, *34*, 1924−1933. (p) Auburn, P. R.; Lever, A. B. P. *Inorg. Chem.* **1990**, *29*, 2551−2553. (q) Metcalfe, R. A.; Vasconcellos, L. C. G.; Mirza, H.; Franco, D. W.; Lever, A. B. P. *J. Chem. Soc., Dalton Trans.* **1999**, 2653−2667. (r) Shukla, A.; Das, A. *Polyhedron* **2000**, *19*, 2605−2611. (s) Ward, M. D. *Inorg. Chem.* **1996**, *35*, 1712−1714. (t) Dei, A.; Gatteschi, D.; Pardi, L. *Inorg. Chem.* **1990**, *29*, 1442−1444. (u) Bruni, S.; Cariati, F.; Dei, A.; Gatteschi, D. *Inorg. Chim. Acta* **1991**, *186*, 157−160. (v) Joulie, L. F.; Schatz, E.; Ward, M. D.; Weber, F.; Yellowless, L. J. *J. Chem. Soc., Dalton Trans.* **1994**, 799−804. (w) Joss, S.; Reust, H.; Ludi, A. *J. Am. Chem. Soc.* **1981**, *103*, 981−982.

(6) (a) Keene, F. R. *Chem. Soc. Rev.* **1998**, *27*, 185. (b) D'Alessandro, D. M.; Keene, F. R. *Chem. Phys.* **2006**, *324*, 8−25.

(7) Gooden, V. M.; Dasgupta, T. P.; Gordon, N. R.; Sadler, G. G. *Inorg. Chim. Acta* **1998**, *268*, 31−36.

(8) (a) Sarkar, B.; Patra, S.; Fiedler, J.; Sunoj, R. B.; Janardanan, D.; Mobin, S. M.; Niemeyer, M.; Lahiri, G. K.; Kaim, W. *Angew. Chem., Int. Ed.* **2005**, *44*, 5655−5658. (b) Sarkar, B.; Patra, S.; Fiedler, J.; Sunoj, R. B.; Janardanan, D.; Lahiri, G. K.; Kaim, W. *J. Am. Chem. Soc.* **2008**, *130*, 3532−3542.

(9) (a) Patra, S.; Sarkar, B.; Ghumaan, S.; Fiedler, J.; Kaim, W.; Lahiri, G. K. *Inorg. Chem.* **2004**, *43*, 6108−6113. (b) Patra, S.; Sarkar, B.; Ghumaan, S.; Fiedler, J.; Kaim, W.; Lahiri, G. K. *Dalton Trans.* **2004**, 754−758. (c) Kar, S.; Chanda, N.; Mobin, S. M.; Datta, A.; Urbanos, F. A.; Puranik, V. G.; Jimenez-Aparicio, R.; Lahiri, G. K. *Inorg. Chem.* **2004**, *43*, 4911−4920. (d) Ghumaan, S.; Sarkar, B.; Patra, S.; Parimal, K.; Slageren, J. V.; Fiedler, J.; Kaim, W.; Lahiri, G. K. *Dalton Trans.* **2005**, 706−712. (e) Patra, S.; Miller, T. A.; Sarkar, B.; Niemeyer, M.; Ward, M. D.; Lahiri, G. K. *Inorg. Chem.* **2003**, *42*, 4707−4713. (f) Patra, S.; Mondal, B.; Sarkar, B.; Niemeyer, M.; Lahiri, G. K. *Inorg. Chem.* **2003**, *42*, 1322−1327. (g) Kar, S.; Chanda, N.; Mobin, S. M.; Urbanos, F. A.; Niemeyer, M.; Puranik, V. G.; Jimenez-Aparicio, R.; Lahiri, G. K. *Inorg. Chem.* **2005**, *44*, 1571−1579. (h) Maji, S.; Sarkar, B.; Patra, S.; Fiedler, J.; Mobin, S. M.; Puranik, V. G.; Kaim, W.; Lahiri, G. K. *Inorg. Chem.* **2006**, *45*, 1316−1325.

(10) (a) Das, A.; Scherer, T.; Maji, S.; Mondal, T. K.; Mobin, S. M.; Urbanos, F. A.; Jiménez-Aparicio, R.; Kaim, W.; Lahiri, G. K. *Inorg. Chem.* **2011**, *50*, 7040−7049. (b) Koiwa, T.; Masuda, Y.; Shono, J.; Kawamoto, Y.; Hoshino, Y.; Hashimoto, T.; Natarajan, K.; Shimizu, K. *Inorg. Chem.* **2004**, *43*, 6215−6223. (c) Eaton, D. R. *J. Am. Chem. Soc.* **1965**, *87*, 3097−3102. (d) Palmer, R. A.; Fay, R. C.; Piper, T. S. *Inorg. Chem.* **1964**, *3*, 875−881. (e) Holm, R. H.; Cotton, F. A. *J. Am. Chem. Soc.* **1958**, *80*, 5658−5663. (f) Fay, R. C.; Piper, T. S. *J. Am. Chem. Soc.* **1963**, *85*, 500−504. (g) Chen, J.-L.; Zhang, X.-U.; Zhang, L.-Y.; Shi, L.-X.; Chen, Z.-N. *Inorg. Chem.* **2005**, *44*, 1037−1043.

(11) (a) Hashimoto, T.; Hara, S.; Shiraishi, Y.; Natarajan, K.; Shimizu, K. *Chem. Lett.* **2003**, *32*, 874−875. (b) Hashimoto, T.; Hara, S.; Shiraishi, Y.; Yamauchi, M.; Natarajan, K.; Shimizu, K. *Inorg. Chim. Acta* **2005**, *358*, 2207−2216.

(12) Chao, G. K. J.; Sime, R. L.; Sime, R. J. *Acta Crystallogr.* **1973**, *B29*, 2845−2849.

(13) Kundu, T.; Chowdhury, A. D.; De, D.; Mobin, S. M.; Dutta, A.; Lahiri, G. K. *Dalton Trans.* **2012**, *41*, 4484−4496.

(14) (a) Levin, E. M. *J. Magn. Mater.* **2013**, *340*, 113−119. (b) Yoon, J. H.; Lee, W. R.; Ryu, D. W.; Lee, J. W.; Yoon, S. W.; Suh, B. J.; Kim, H. C.; Hong, C. S. *Inorg. Chem.* **2011**, *50*, 10777−10785. (c) Jia, H.-P.; Li, W.; Ju, Z.-F.; Zhang, J. *Chem. Commun.* **2008**, 371−373. (d) Huang, Y.-G.; Yuan, D.-Q.; Pan, L.; Jiang, F.-L.; Wu, M.-Y.; Zhang, X.-D.; Wei, W.; Gao, Q.; Lee, J. Y.; Li, J.; Hong, M.-C. *Inorg. Chem.* **2007**, *46*, 9609−9615.

(15) Creutz, C. *Prog. Inorg. Chem.* **1983**, *30*, 1−73.

(16) (a) Richardson, D. E.; Taube, H. *Coord. Chem. Rev.* **1984**, *60*, 107−129. (b) Evans, C. E. B.; Naklicki, M. L.; Rezvani, A. R.; White, C. A.; Kondratiev, V. V.; Crutchley, R. J. *J. Am. Chem. Soc.* **1998**, *120*, 13096−13103. (c) Creutz, C.; Newton, M. D.; Sutin, N. *J. Photochem. Photobiol., A* **1994**, *82*, 47−59.

(17) Mandal, A.; Kundu, T.; Ehret, F.; Bubrin, M.; Mobin, S. M.; Kaim, W.; Lahiri, G. K. *Dalton Trans.* **2014**, *43*, 2473−2487.

(18) Sadler, G. G.; Gordon, N. R. *Inorg. Chim. Acta* **1991**, *180*, 271−276.

(19) Weil, J. A.; Bolton, J. R. *Electron Paramagnetic Resonance*, 2nd ed.; Wiley: Hoboken, 2007.

(20) Kaim, W. *Coord. Chem. Rev.* **2011**, *255*, 2503−2513.

(21) Robin, M. B.; Day, P. *Adv. Inorg. Chem. Radiochem.* **1967**, *10*, 247−422.

(22) Kaim, W.; Sarkar, B. *Coord. Chem. Rev.* **2013**, *257*, 1650−1659.

(23) Ernst, S. D.; Kaim, W. *Inorg. Chem.* **1989**, *28*, 1520−1528.

(24) Kobayashi, T.; Nishina, Y.; Shimizu, K. G.; Satô, G. P. *Chem. Lett.* **1988**, 1137−1140.

(25) Sullivan, B. P.; Salmon, D. J.; Meyer, T. J. *Inorg. Chem.* **1978**, *17*, 3334−3341.

(26) Kaim, W.; Ernst, S.; Kasack, V. *J. Am. Chem. Soc.* **1990**, *112*, 173−178.

(27) Krejcik, M.; Danek, M.; Hartl, F. *J. Electroanal. Chem.* **1991**, *317*, 179−187.

(28) (a) Sheldrick, G. M. *Acta Crystallogr., Sect. A* **2008**, *A64*, 112−122. (b) *Program for Crystal Structure Solution and Refinement*; University of Göttingen: Göttingen, Germany, 1997.

(29) Lee, C.; Yang, W.; Parr, R. G. *Phys. Rev. B* **1988**, *37*, 785−789.

(30) (a) Andrae, D.; Haeussermann, U.; Dolg, M.; Stoll, H.; Preuss, H. *Theor. Chim. Acta* **1990**, *77*, 123−141. (b) Fuentealba, P.; Preuss, H.; Stoll, H.; Szentpaly, L. V. *Chem. Phys. Lett.* **1989**, *89*, 418−422.

(31) Frisch, M. J.; Trucks, G. W.; Schlegel, H. B.; Scuseria, G. E.; Robb, M. A.; Cheeseman, J. R.; Scalmani, G.; Barone, V.; Mennucci, B.; Petersson, G. A.; Nakatsuji, H.; Caricato, M.; Li, X.; Hratchian, H. P.; Izmaylov, A. F.; Bloino, J.; Zheng, G.; Sonnenberg, J. L.; Hada, M.; Ehara, M.; Toyota, K.; Fukuda, R.; Hasegawa, J.; Ishida, M.; Nakajima, T.; Honda, Y.; Kitao, O.; Nakai, H.; Vreven, T.; Montgomery Jr., J. A.; Peralta, J. E.; Ogliaro, F.; Bearpark, M.; Heyd, J. J.; Brothers, E.; Kudin, K. N.; Staroverov, V. N.; Kobayashi, R.; Normand, J.; Raghavachari, K.; Rendell, A.; Burant, J. C.; Iyengar, S. S.; Tomasi, J.; Cossi, M.; Rega, N.; Millam, J. M.; Klene, M.; Knox, J. E.; Cross, J. B.; Bakken, V.; Adamo, C.; Jaramillo, J.; Gomperts, R.; Stratmann, R. E.; Yazyev, O.; Austin, A. J.; Cammi, R.; Pomelli, C.; Ochterski, J. W.; Martin, R. L.; Morokuma, K.; Zakrzewski, V. G.; Voth, G. A.; Salvador, P.; Dannenberg, J. J.; Dapprich, S.; Daniels, A. D.; Farkas, O.;

Foresman, J. B.; Ortiz, J. V.; Cioslowski, J.; Fox, D. J. *Gaussian 09 (Revision A.02)*; Gaussian, Inc.: Wallingford, CT, 2009.
(32) (a) Bauernschmitt, R.; Ahlrichs, R. *Chem. Phys. Lett.* **1996**, *256*, 454−464. (b) Stratmann, R. E.; Scuseria, G. E.; Frisch, M. J. *J. Chem. Phys.* **1998**, *109*, 8218−8225. (c) Casida, M. E.; Jamorski, C.; Casida, K. C.; Salahub, D. R. *J. Chem. Phys.* **1998**, *108*, 4439−4450.
(33) (a) Barone, V.; Cossi, M. *J. Phys. Chem. A* **1998**, *102*, 1995−2001. (b) Cossi, M.; Barone, V. *J. Chem. Phys.* **2001**, *115*, 4708−4718. (c) Cossi, M.; Rega, N.; Scalmani, G.; Barone, V. *J. Comput. Chem.* **2003**, *24*, 669−681.
(34) Leonid, S. *Chemissian 1.7*; 2005−2010. Available at http://www.chemissian.com.
(35) Zhurko, D. A.; Zhurko, G. A. *ChemCraft 1.5*; Plimus: San Diego, CA. Available at http://www.chemcraftprog.com.

dx.doi.org/10.1021/ic500452h | *Inorg. Chem.* 2014, 53, 6082−6093